Int. J. Heat Mass Transfer. Vol. 30, No. 11, pp. 2373–2383, 1987
Printed in Great Britain

0017-9310/87 $3.00 + 0.00

Effects of radial thermal dispersion on fully-developed forced convection in cylindrical packed tubes

P. CHENG and H. ZHU
Department of Mechanical Engineering, University of Hawaii at Manoa, Honolulu, HI 96822, U.S.A.

(*Received* 20 *January* 1987 *and in final form* 15 *April* 1987)

Abstract—The fluid flow and heat transfer characteristics of a fully-developed forced convective flow in a cylindrical packed tube with symmetric heating are analyzed in this paper. The Darcy–Brinkman–Ergun model is used as the momentum equation, with the radial porosity variation of the packed column approximated by an exponential function. The method of matched asymptotic expansions is applied to construct a composite solution for the axial velocity profile of a hydrodynamically fully-developed flow. The interaction of inertial and wall channeling effects on the pressure drop and the axial velocity profile is illustrated. The effects of radial thermal dispersion and variable stagnant thermal conductivity are taken into consideration in the energy equation for a thermally fully-developed flow in the packed tube, which is heated circumferentially with constant heat flux or constant wall temperature. A wall function is used to model the wall effect on the transverse thermal dispersion process, and the predicted Nusselt numbers agree with existing experimental data. Numerical results of the corresponding heat transfer characteristics in the packed tubes, without introducing the wall function, are also presented for comparison.

1. INTRODUCTION

DURING the past 50 years, a considerable amount of experimental work has been performed on forced convection in packed columns [1, 2]. The purpose of these experiments was to obtain correlation equations of the effective thermal conductivity and heat transfer rate for the design of wall-cooled catalytic reactors. From the early experimental data, it was observed that steep radial temperature gradients, resembling a temperature discontinuity, usually exist in a packed column near a heated or cooled wall [3, 4]. To account for the localized thermal resistance near the wall, Coberly and Marshall [5] introduced the concept of a wall heat transfer coefficient h_w which is defined as

$$-k_{er}^{*}\left(\frac{\partial T^{*}}{\partial r^{*}}\right)_{r^{*}=r_0^{*}} = h_w(T_w^{*}-T^{*})_{r^{*}=r_0^{*}} \qquad (1)$$

where T_w^{*} is the wall temperature, r_0^{*} the radius of the packed column, and k_{er}^{*} is the effective radial thermal conductivity of the packed bed. The values of k_{er}^{*} and h_w (both assumed to be constant and independent of position) as a function of the Reynolds number Re_d (based on particle diameter d_p) were determined simultaneously by matching the temperature data with a theoretical model that assumes a plug flow (i.e. a flat velocity profile) with the thermal boundary condition given by equation (1). The radial variations in the thermal conductivity, axial velocity and porosity near the wall are lumped together and accounted for by a wall heat transfer coefficient in equation (1)—hence the name 'lumped parameter model'. Using this method for the analysis of experimental data, it was found while the effective radial thermal conductivity can be correlated as a linear function of Re_d, the exponent of Re_d in the correlation equation for the Nusselt number ranges from 0.33 to 1.0 as reported by different investigators [1, 2].

The lumped parameter model has been widely used for the simulation of the performance of wall-cooled catalytic reactors. Recent studies, however, show that these numerical models often over-predict the temperature of hot spots in the reactors [6, 7]. The disparity of the predicted and experimentally determined temperature distributions in these wall-cooled catalytic reactors has been attributed to the unrealistic assumption of a constant effective radial thermal conductivity in the lumped parameter model, and the widely scattered correlation equations for the wall heat transfer coefficient used in equation (1).

The fact that the local effective radial thermal conductivity is reduced drastically near the wall is well known since the early experiment conducted by Kwong and Smith [8]. Thus, in the recent numerical models by Finlayson [9] and by Botterill and Denloye [10], a reduced value of k_{er}^{*} within $\frac{1}{2}d_p$ away from the wall is used. As a result, the concept of a wall heat transfer coefficient is not needed and the artificial boundary condition given by equation (1) need not be imposed. This is the so-called 'distributed parameter model' for the simulation of the performance of a wall-cooled catalytic reactor in the chemical engineering literature. In a most recent model by Ahmed

NOMENCLATURE

a	empirical constant in equations (4)
b	empirical constant in equation (4b)
B_0	function defined in equation (50b)
c_p	specific heat at constant pressure
c_∞	constant defined in equation (10)
C_1	empirical constant in equation (3)
d_p	particle diameter
D	diameter of the tube
D_T	empirical constant defined in equation (51)
F	normalized coefficient of inertia defined in equation (7)
F^*	coefficient of inertia defined in equation (4b)
F_∞^*	coefficient of inertia at infinity
$\hat{F}$	coefficient of inertia in the inner solution
$\hat{F}_0, \hat{F}_1$	first- and second-order coefficient of inertia in the inner solution
h	heat transfer coefficient defined in equation (44)
h_w	heat transfer coefficient defined in equation (1)
K	normalized permeability defined in equation (7)
K^*	permeability
K_∞^*	permeability at the core
$\hat{K}$	inner permeability function
$\hat{K}_0, \hat{K}_1$	first- and second-order inner permeability function
k_d^*	stagnant thermal conductivity of the packed bed
k_f^*	thermal conductivity of the fluid phase
k_s^*	thermal conductivity of the solid phase
k_T^*	thermal dispersion conductivity
k_{er}^*	effective thermal conductivity in the radial direction
k_{er}	dimensionless effective thermal conductivity in the radial direction
l	wall function for transverse thermal dispersion
L	length of the packed tube
N	inertial parameter in equation (8)
N_1	empirical constant in equation (3)
Nu_d	Nusselt number defined in equation (45)
p^*	pressure
Pr	Prandtl number of the fluid
q_w	heat flux at the wall
R	dimensionless outer radial coordinate defined in equation (16)
$\hat{R}$	dimensionless outer radial coordinate defined in equation (24)
r^*	radial coordinate
r	dimensionless radial coordinate
r_0^*	radius of the cylindrical packed column
r_0	dimensionless radius of the packed column
Re_d	Reynolds number defined in equation (36)
Re_∞	Reynolds number based on u_∞^*
T^*	temperature
T_b^*	bulk temperature
T_w^*	wall temperature
U	dimensionless outer velocity defined in equation (16)
U_0, U_1	first- and second-order outer velocity
u	dimensionless axial velocity defined in equation (7)
u_m	dimensionless mean velocity defined in equation (38)
u^*	axial velocity
u_∞^*	axial velocity at the center of the packed tube
u_m^*	mean velocity
$\hat{u}$	dimensionless inner velocity
$\hat{u}_0, \hat{u}_1$	first- and second-order inner velocities
x^*	axial coordinate.

Greek symbols

α_∞	dimensionless pressure gradient based on u_∞^*
α_m	dimensionless pressure gradient based on u_m^*
Γ	constant defined in equation (34)
γ	ratio of particle diameter to radius of the packed column
ε	small parameter, σ/γ
θ	dimensionless temperature defined in equation (41)
Λ	thermal conductivity ratio of the solid phase to fluid phase
μ^*	viscosity of the fluid
ρ^*	density of fluid
σ	perturbation parameter in equation (8)
ϕ^*	porosity of the packed bed
ϕ_∞^*	porosity at the core of the packed bed
ϕ	normalized porosity function
$\hat{\phi}$	normalized inner porosity function
$\hat{\phi}_0, \hat{\phi}_1$	first- and second-order inner porosity function
ω	empirical constant in equation (52).

and Fahien [11], the value of k_{er}^* is assumed to vary linearly with the radial distance from the wall to a few particle diameters away from the wall. The predicted heat transfer characteristics are found in good agreement with their experimental data of a catalytic bed.

In a series of papers [12–15], Cheng and co-workers

have analyzed the wall effect on the transverse thermal dispersion process in the forced convective flow through packed columns heated asymmetrically. In these analyses, the no-slip boundary condition and the non-uniform porosity effects have been taken into consideration. In order to match the predicted temperature distribution and the Nusselt number with existing experimental results [16, 17], it was found that a wall function must be introduced to account for the wall effect on the transverse thermal dispersion due to a reduction in the lateral mixing of fluid. Without the introduction of the wall function, the large temperature gradient near the heated wall as observed from experiments cannot be reproduced.

In this paper, the fluid flow and heat transfer characteristics of a fully-developed forced convective flow in cylindrical packed tubes with symmetric heating are analyzed. The Darcy–Brinkman–Ergun model [18] is used as the momentum equation, with the radial porosity variation approximated by an exponential function. The effects of inertia and wall channeling on the pressure drop and the axial velocity profile are illustrated. The effects of transverse thermal dispersion and the variable stagnant thermal conductivity are taken into consideration in the energy equation for a thermally fully-developed flow in a cylindrical packed tube heated with constant heat flux or constant wall temperature. If a wall function is used to model the wall effect on the transverse thermal dispersion process, the predicted Nusselt numbers are found in agreement with experimental data [19, 20]. Numerical results of the corresponding heat transfer characteristics in the packed tube, without introducing the wall function, are also presented for comparison purposes.

2. HYDRODYNAMICALLY FULLY-DEVELOPED FLOW IN A PACKED TUBE

Consider a steady incompressible flow through a cylindrical packed tube with radius r_0^*. If the flow is considered to be hydrodynamically fully developed, the momentum equation based on the Darcy–Brinkman–Ergun model in a cylindrical coordinate system (x^*, r^*) is [18]

$$\frac{\mu^* u^*}{K^*} + \frac{\rho^* F^* u^{*2}}{\sqrt{K^*}} = -\frac{\mathrm{d}p^*}{\mathrm{d}x^*} + \frac{\mu^*}{\phi^*}\frac{1}{r^*}\frac{\mathrm{d}}{\mathrm{d}r^*}\left(r^*\frac{\mathrm{d}u^*}{\mathrm{d}r^*}\right) \tag{2}$$

where u^* is the velocity in the x^*-direction (i.e. the axial direction), $\mathrm{d}p^*/\mathrm{d}x^*$ is the externally imposed pressure gradient, and ρ^* and μ^* are the density and axial viscosity of the fluid. ϕ^* is the porosity of the packed column which can be approximated by an exponential function of the form [21]

$$\phi^* = \phi_\infty^* \left\{1 + C_1 \exp\left[-\frac{N_1(r_0^* - r^*)}{d_p}\right]\right\} \tag{3}$$

where d_p is the parameter diameter, $C_1 = 1$, $N_1 = 2$, and $\phi_\infty^* = 0.4$ is the porosity at the core of the packed column. For a packed-sphere bed, the permeability K^* and the dimensionless inertial coefficient are given by [18]

$$K^* = \frac{\phi^{*3} d_p^2}{a(1-\phi^*)^2} \quad \text{and} \quad F^* = \frac{b}{\sqrt{a}\phi^{*3/2}} \tag{4a,b}$$

where $a = 150$ and $b = 1.75$ are the empirical constants [22]. The boundary conditions for equation (2) are

$$r^* = 0: \quad u^* = u_\infty^* \tag{5}$$

$$r^* = r_0^*: \quad u^* = 0 \tag{6}$$

where u_∞^* is the velocity in the core of the packed column.

We now define the following normalized variables:

$$u = u^*/u_\infty^*, \quad \phi = \phi^*/\phi_\infty^*, \quad K = K^*/K_\infty^*, \quad F = F^*/F_\infty^*, \quad r = r^*/d_p \tag{7}$$

where

$$K_\infty^* = \phi_\infty^{*3} d_p^2/a(1-\phi_\infty^*)^2$$

and

$$F_\infty^* = \frac{b}{(\sqrt{a}\phi_\infty^{*3/2})}.$$

Equations (2)–(6) in terms of the normalized variables are

$$\frac{u}{K} + \frac{NFu^2}{\sqrt{K}} = \alpha_\infty + \frac{\sigma^2}{\phi r}\frac{\mathrm{d}}{\mathrm{d}r}\left(r\frac{\mathrm{d}u}{\mathrm{d}r}\right) \tag{8}$$

$$\phi = 1 + C_1 \exp\left[-N_1(r_0 - r)\right] \tag{9}$$

$$K = \frac{\phi^3}{[1 + c_\infty(1-\phi)]^2} \tag{10}$$

$$F = \phi^{-3/2} \tag{11}$$

subject to the boundary conditions

$$r = 0: \quad u = 1 \tag{12}$$

$$r = 1/\gamma: \quad u = 0 \tag{13}$$

where

$$\alpha_\infty = -\frac{K_\infty^*}{\mu^* u_\infty^*}\left(\frac{\mathrm{d}p^*}{\mathrm{d}x^*}\right)$$

$$N = Re_\infty\left[\frac{b}{a(1-\phi_\infty^*)}\right]$$

with

$$Re_\infty = \rho^* u_\infty^* d_p/\mu^*$$

$$\gamma = d_p/r_0^*, \quad c_\infty = \frac{\phi_\infty^*}{1-\phi_\infty^*}$$

$$\sigma = \sqrt{\left(\frac{K_\infty^*}{\phi_\infty^*}\right)}\Big/ d_p = c_\infty/\sqrt{a} = 0.0544$$

if $\phi_\infty^* = 0.4$ and $a = 150$.

Since the dimensionless pressure drop α_∞ is a constant (independent of r), we can determine its value in the core region. In the core region ($r = 0$) where the boundary friction effect is negligible and $u = \phi = F = K = 1$, equation (8) becomes

$$1 + N = \alpha_\infty. \tag{14}$$

Substituting equation (14) into equation (8) yields

$$\frac{u}{K} + \frac{NFu^2}{\sqrt{K}} = 1 + N + \frac{\sigma^2}{\phi r}\frac{\mathrm{d}}{\mathrm{d}r}\left(r\frac{\mathrm{d}u}{\mathrm{d}r}\right). \tag{15}$$

We now attempt to solve equation (15) and (9)–(11) subject to boundary conditions (12) and (13) by the method of matched asymptotic expansions under the conditions $\sigma \ll 1$, $\gamma < 1$ and $\varepsilon = \sigma/\gamma \ll 1$.

2.1. *The outer solution*

For the variable porosity layer (i.e. the outer layer), the following outer variables are defined:

$$R = (r_0^* - r^*)/d_p = (r_0 - r) \quad \text{and} \quad U = u \tag{16}$$

where $r_0 = r_0^*/d_p$. Equations (15) and (9) in terms of the outer variables become

$$\frac{U}{K} + \frac{NFU^2}{\sqrt{K}} = 1 + N + \frac{\sigma^2}{\phi(r_0 - R)}\frac{\mathrm{d}}{\mathrm{d}R}\left[(r_0 - R)\frac{\mathrm{d}U}{\mathrm{d}R}\right] \tag{17}$$

$$\phi = 1 + C_1 \exp[-N_1 R]. \tag{18}$$

Equations (17) and (18) with equations (10) and (11) are to be solved subject to the boundary condition

$$R \to \infty: \quad U = 1 \tag{19}$$

and $R \to 0$, the outer solution must match with the inner solution.

We now assume the following series expansions for the outer variable U:

$$U = U_0 + \sigma U_1 + O(\sigma^2). \tag{20}$$

Substituting equation (20) into equation (17) yields the following first-order outer problem:

$$\frac{U_0}{K} + \frac{NFU_0^2}{\sqrt{K}} = 1 + N \tag{21}$$

with the boundary condition given by

$$R \to \infty: \quad U_0 = 1 \tag{22}$$

and $R \to 0$, U_0 must match with the first-order inner solution. Equation (21) can be readily solved to give

$$U_0(R) = \frac{-\dfrac{1}{K} + \sqrt{\left(\dfrac{1}{K^2} + \dfrac{4N(1+N)F}{\sqrt{K}}\right)}}{\dfrac{2NF}{\sqrt{K}}} \tag{23}$$

where F and K are given by equations (10) and (11). The positive sign in front of the square root of equation (23) has been chosen so that boundary condition (22) can be satisfied. It is relevant to note that equation (23) is identical to the first-order outer solution of a hydrodynamically fully-developed flow in a rectangular packed channel [15]. This implies that, to the first-order, the geometry of the packed column has no effect on the outer solution.

2.2. *The inner solution*

As in the previous work [15], the following inner variables will now be introduced:

$$\hat{R} = \frac{\sqrt{(1+N)}}{\sigma}R = \frac{\sqrt{(1+N)}}{\sigma}(r_0 - r),$$

$$\hat{u} = u, \quad \hat{\phi} = \phi, \quad \hat{F} = F, \quad \hat{K} = K. \tag{24}$$

In terms of the above inner variables, equations (9) and (15) become

$$\hat{\phi} = 1 + C_1 \exp\left[-\frac{\sigma N_1 \hat{R}}{\sqrt{(1+N)}}\right] \tag{25}$$

$$\frac{\hat{u}}{\hat{K}} + \frac{N\hat{F}\hat{u}^2}{\sqrt{\hat{K}}} = (1+N) + \frac{1+N}{\hat{\phi}\left[r_0 - \dfrac{\sigma\hat{R}}{\sqrt{(1+N)}}\right]}\frac{\mathrm{d}}{\mathrm{d}\hat{R}} \times \left[\left(r_0 - \frac{\sigma\hat{R}}{\sqrt{(1+N)}}\right)\frac{\mathrm{d}\hat{u}}{\mathrm{d}\hat{R}}\right] \tag{26}$$

which are to be solved subject to the boundary condition

$$\hat{R} = 0: \quad \hat{u} = 0 \tag{27}$$

and the matching condition from the outer solution.

We now assume the following series expansions for the inner variables:

$$\begin{aligned} \hat{u} &= \hat{u}_0 + \sigma\hat{u}_1 + O(\sigma^2) \\ \hat{\phi} &= \hat{\phi}_0 + \sigma\hat{\phi}_1 + O(\sigma^2) \\ \hat{K} &= \hat{K}_0 + \sigma\hat{K}_1 + O(\sigma^2) \\ \hat{F} &= \hat{F}_0 + \sigma\hat{F}_1 + O(\sigma^2). \end{aligned} \tag{28}$$

Substituting equations (28) into equations (25)–(27), (10) and (11) gives the following first-order inner problem:

$$\hat{\phi}_0 = 1 + C_1 \tag{29}$$

$$\hat{K}_0 = \frac{\hat{\phi}_0^3}{[1 + C_\infty(1 - \hat{\phi}_0)]^2} \tag{30}$$

$$\hat{F}_0 = \hat{\phi}_0^{-3/2} \tag{31}$$

$$\frac{\hat{u}_0}{\hat{K}_0} + \frac{N\hat{F}_0\hat{u}_0^2}{\sqrt{\hat{K}_0}} = (1+N) + \frac{(1+N)}{\hat{\phi}_0\left[r_0 - \dfrac{\sigma\hat{R}}{\sqrt{(1+N)}}\right]}\frac{\mathrm{d}}{\mathrm{d}\hat{R}} \times \left[\left(r_0 - \frac{\sigma\hat{R}}{\sqrt{(1+N)}}\right)\frac{\mathrm{d}\hat{u}_0}{\mathrm{d}\hat{R}}\right] \tag{32}$$

with boundary conditions given by

$$\hat{u}_0(0) = 0 \tag{33}$$

and the matching condition

$$\hat{R} \to \infty: \quad \hat{u}_0(\hat{R}) = \Gamma$$

where

$$\Gamma = U_0(0) = \frac{-\frac{1}{\hat{K}_0} + \sqrt{\left(\frac{1}{\hat{K}_0^2} + \frac{4N(1+N)}{\sqrt{K_0}}\hat{F}_0\right)}}{2N\hat{F}_0/\sqrt{\hat{K}_0}} \tag{34}$$

which is obtained from the outer solution given by equation (23) by letting $R \to 0$. Numerical solutions of equations (29)–(34) can be obtained by the Runge–Kutta method.

A composite solution for the axial velocity can be constructed from the first-order inner and outer solutions based on the multiplicative rule [23] as follows:

$$u = \frac{U_0(R)\hat{u}_0(\hat{R})}{\Gamma} + O(\sigma) \tag{35}$$

where $U_0(R)$ is given by equation (23) and $\hat{u}_0(\hat{R})$ is given by equations (29)–(34) which are functions of Re_∞. However, it will be more meaningful to express the results in terms of a Reynolds number based on the mean velocity u_m^*, i.e.

$$Re_d = u_m^* d_p/\nu = Re_\infty u_m \tag{36}$$

where u_m^* and u_m are dimensional and dimensionless mean velocities defined as

$$u_m^* = \frac{2}{r_0^{*2}}\int_0^{r_0^*} r^* u^* \, dr^* \tag{37}$$

and

$$u_m = \frac{u_m^*}{u_\infty^*} = 2\gamma^2 \int_0^{1/\gamma} ru \, dr. \tag{38}$$

Equation (38) shows that u_m is a function of both Re_d and γ. It follows from the definitions that the normalized axial velocity is given by

$$u^*/u_m^* = u/u_m \tag{39}$$

where u is given by equation (35) and u_m is given by equation (38). The normalized velocity given by equation (39) vs the normalized coordinate $(r_0-r)/r_0$ is plotted in Fig. 1 for a variable-porosity cylindrical packed column with $\gamma = 0.03$ and 0.37 at different values of Re_d. The dashed lines represent the normalized axial velocity without inertial effect ($b = 0$), while the solid lines represent those with inertial effect. As in the previous work [15], the velocity overshoot occurs at a distance about $0.1d_p$–$0.15d_p$ away from the wall. The peak velocity decreases as the value of γ is increased. It is interesting to note that the shape of the axial profile depends on the value of Re_d for $Re_d < 100$, but is relatively independent of Re_d for $Re_d > 100$.

The wall channeling effect on pressure drop will be considered next. The dimensionless pressure gradient based on the mean velocity is given by

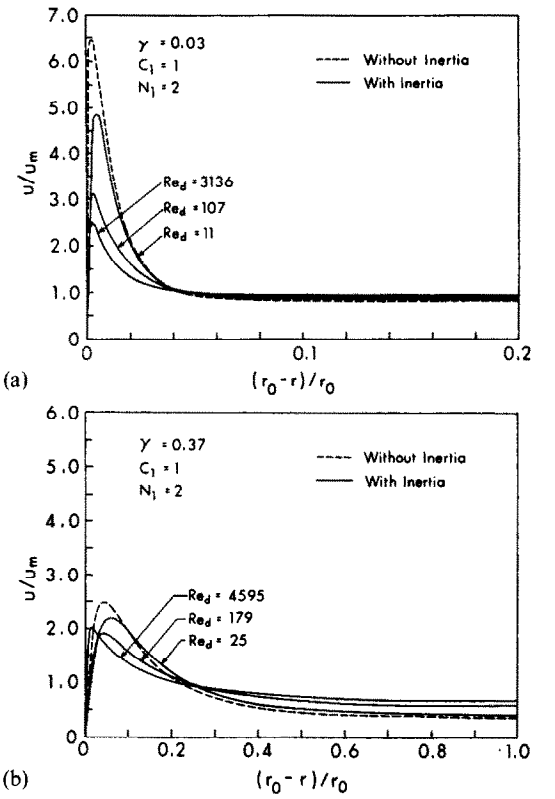

FIG. 1. Effects of wall channeling and inertia on dimensionless axial velocity in a packed tube: (a) $\gamma = 0.03$; (b) $\gamma = 0.37$.

$$\alpha_m = -\frac{K_\infty^*}{\mu^* u_m^*}\frac{dp^*}{dx^*} = \frac{\alpha_\infty}{u_m} = (1+N)/u_m \tag{40}$$

where u_m is given by equation (38). Equation (40) is plotted as solid lines in Fig. 2 as a function of Re_d at three values of γ ($\gamma = 0.03$, 0.074 and 0.37). For comparison the pressure gradient in a constant porosity ($C_I = 0$) cylindrical packed column is plotted as dashed lines. As in the previous work [15], the wall channeling effect on pressure gradient is more pronounced in the Darcy and Forchheimer flow regions ($Re_d < 100$) than in the turbulent flow region ($Re_d > 100$).

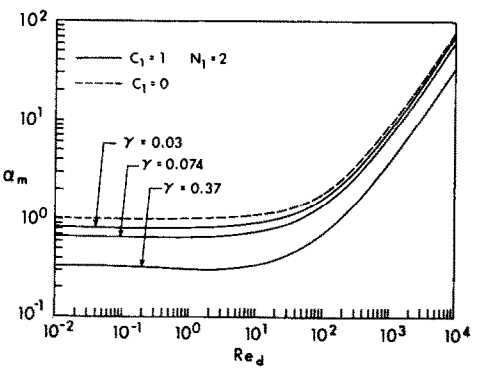

FIG. 2. Effects of wall channeling on dimensionless pressure gradient in a packed tube.

3. THERMALLY FULLY-DEVELOPED FORCED CONVECTION IN A PACKED TUBE

A thermally fully-developed flow in a tube with symmetric heating is defined as [24]

$$\frac{\partial\theta}{\partial x^*} = 0 \tag{41}$$

where

$$\theta = \frac{T_w^* - T^*(x^*, r^*)}{T_w^* - T_b^*(x^*)}$$

with T_w^* denoting the wall temperature and T_b^* the bulk temperature defined as

$$T_b^*(x^*) = \frac{2\int_0^{r_0^*} T^* r^* u^* \, dr^*}{u_m^* r_0^{*2}}. \tag{42}$$

The conservation of energy from a differential control volume gives [24]

$$\frac{dT_b^*}{dx^*} = \frac{2q_w}{\rho u_m^* c_p r_0^*} \tag{43}$$

where q_w is the heat flux at the wall, which is related to the heat transfer coefficient by

$$q_w = h(T_w^* - T_b^*). \tag{44}$$

The Nusselt number for the present problem is defined as

$$Nu_d = \frac{hd_p}{k_f^*} = \frac{q_w d_p}{k_f^*(T_w^* - T_b^*)} \tag{45}$$

where k_f^* is the thermal conductivity of the fluid and

$$(T_w^* - T_b^*) = \frac{2}{u_m^* r_0^{*2}} \int_0^{r_0^*} (T_w^* - T^*) r^* u^* \, dr^* \tag{46}$$

which is obtained from equations (37) and (42).

Equations (41)–(46) are applicable for a thermally fully-developed forced convective flow in a cylindrical packed tube with constant heat flux or constant wall temperature. The heat transfer characteristics of these two cases will now be considered separately.

3.1. *Constant heat flux*

For a thermally fully-developed flow with constant heat flux, it can be shown that [24]

$$\frac{\partial T^*}{\partial x^*} = \frac{dT_b^*(x^*)}{dx^*} = \frac{dT_w^*(x^*)}{dx^*} = \frac{2q_w}{(\rho c_p)_f r_0^* u_m^*} \tag{47}$$

where q_w is a constant. With the aid of the above equation, the energy equation becomes

$$\frac{u^*}{u_m^*}\frac{2q_w}{r_0^*} = \frac{1}{r^*}\frac{d}{dr^*}\left(r^* k_{er}^* \frac{dT^*}{dr^*}\right) \tag{48}$$

where k_{er}^* is the effective radial thermal conductivity which is defined as

$$k_{er}^* = k_d^* + k_T^*. \tag{49}$$

In the above equation, k_d^* is the stagnant thermal conductivity of the packed column which is given by the following semi-analytical expression [25]

$$\frac{k_d^*}{k_f^*} = 1 - \sqrt{(1-\phi^*)} + \frac{2\Lambda\sqrt{(1-\phi^*)}}{(\Lambda - B_0)} \times \left[\frac{B_0\Lambda(\Lambda-1)}{(\Lambda-B_0)^2}\ln\left(\frac{\Lambda}{B_0}\right) - \frac{B_0+1}{2} - \frac{\Lambda(B_0-1)}{\Lambda - B_0}\right] \tag{50a}$$

where

$$B_0 = 1.25\left(\frac{1-\phi^*}{\phi^*}\right)^{10/9} \quad \text{(for spherical particles)} \tag{50b}$$

and

$$\Lambda = k_s^*/k_f^* \tag{50c}$$

with k_s^* denoting the thermal conductivity of the solid particles. The quantity k_T^* in equation (49) is the thermal dispersion conductivity which is given by [14]

$$k_T^*/k_f^* = D_T \, Pr \, Re_d \, ul \tag{51}$$

where D_T is an empirical constant, Pr is the Prandtl number of the fluid, and l is Van Driest's wall function for radial thermal dispersion which is given by [14]

$$l = 1 - e^{-(r_0^* - r^*)/\omega d_p} \tag{52}$$

where ω is an empirical constant. Equation (51) shows that the wall effect on radial thermal dispersion comes from two different sources. First, the presence of a wall modifies the velocity distribution u because of the no-slip boundary condition and the non-uniform porosity effects. Secondly, the presence of a wall would reduce the lateral mixing of fluid which is modeled in terms of a wall function l ($\omega \neq 0$). If the presence of the wall has no effect on lateral mixing, then $\omega = 0$ and $l = 1$.

Equations (48)–(52) are to be solved subject to the boundary conditions

$$r^* = 0: \quad \frac{dT^*}{dr^*} = 0 \tag{53}$$

and

$$r^* = r_0^*: \quad -k_d^*\left(\frac{dT^*}{dr^*}\right) = q_w. \tag{54}$$

Imposing boundary condition (53), equation (48) can be integrated twice to give

$$T^*(x^*, r^*) - T_w^*(x^*) = 2q_w \int_{r_0^*}^{r^*} \frac{1}{r^* k_{er}^*(r^*)} \times \left[\int_0^{r^*} \frac{u^*}{u_m^*} r^* \, dr^*\right] dr^*. \tag{55}$$

Substituting the above equation into equations (46) and (45) yields

$$Nu_d = \frac{1}{4\gamma^3 \int_0^{1/\gamma} \left\{ \int_r^{1/\gamma} \frac{1}{rk_{er}} \left[\int_0^r \frac{ur}{u_m} dr \right] dr \right\} \frac{ru}{u_m} dr} \tag{56}$$

where $k_{er} = k_{er}^*/k_f^*$. With the aid of equations (56) and (45), it can be shown that equation (55) becomes

$$\theta(r) = 2\gamma Nu_d \int_r^{1/\gamma} \frac{1}{rk_{er}} \left[\int_0^r \frac{ur}{u_m} dr \right] dr. \tag{57}$$

For prescribed values of ω, D_T, Re_d, Pr, γ and Λ, equation (56) can be used for the computation of the Nusselt number for a thermally fully-developed forced convective flow in a cylindrical packed tube with constant heat flux. After the value of Nu_d has been determined, equation (57) can be used for the computation of the dimensionless radial temperature distribution in the cylindrical packed tube.

3.2. *Constant wall temperature*

For the case of constant wall temperature, the boundary condition at the wall is given by

$$r^* = r_0^*: \quad T^* = T_w^* \tag{58}$$

and the symmetric boundary condition at the centerline of the tube is given by equation (53). From equations (41) and (45), it can be shown that the energy equation in terms of θ for this case is

$$\frac{1}{r} \frac{d}{dr} \left[rk_{er} \frac{d\theta}{dr} \right] = -2 \left(\frac{u}{u_m} \right) Nu_d \theta \tag{59}$$

with boundary conditions given by

$$r = \frac{1}{\gamma}, \quad \theta = 0 \tag{60}$$

and

$$r = 0, \quad \frac{d\theta}{dr} = 0. \tag{61}$$

Integrating equation (59) twice and imposing boundary conditions (60) and (61) give

$$\theta(r) = 2\gamma Nu_d \int_r^{1/\gamma} \frac{1}{rk_{er}(r)} \left[\int_0^r \theta \left(\frac{u}{u_m} \right) r \, dr \right] dr \tag{62}$$

which is an integral equation for θ. Numerical solutions of equation (62) can be obtained by iteration as follows. For given values of ω, D_T, Re_d, Pr, γ and Λ, u/u_m is obtained from equations (35) and (38), and the first estimated values of $Nu_d^{(i)}$ and $\theta^{(i)}(r)$ can be obtained from the constant heat flux solution given by equations (56) and (57). Substituting these estimated values into the right-hand side of equation (62) gives an improved dimensionless temperature distribution $\theta^{(i+1)}(r)$. The improved value of $Nu_d^{(i+1)}$ can be computed according to

$$Nu_d^{(i+1)} = -\left(k_{er} \frac{d\theta}{dr} \right)_{r=1/\gamma}^{(i)} \tag{63}$$

where

$$\left(k_{er} \frac{d\theta}{dr} \right)_{r=1/\gamma}^{(i)} = -2\gamma^2 Nu_d^{(i)} \int_0^{1/\gamma} \left(\frac{u}{u_m} \right) \theta^{(i)} r \, dr.$$

The iteration process terminates when

$$\left| \frac{Nu_d^{(i+1)} - Nu_d^{(i)}}{Nu_d^{(i+1)}} \right| < 10^{-3}.$$

3.3. *Numerical results and discussion*

Experiments for forced convection of air ($Pr = 0.7$ and $k_f^* = 0.027$ W m^{-1} K^{-1}) in cylindrical packed columns composed of glass spheres ($k_s^* = 1.05$ W m^{-1} K^{-1}) heated circumferentially with constant heat flux or constant wall temperature have been performed by Quinton and Storrow [19] as well as by Verschoor and Schuit [20], respectively. Since air (having a small Prandtl number) was used as the heat transfer medium and since the cylindrical packed tubes used in their experiments have a relatively high length to tube diameter ratio ($L/D = 18.2$ in Quinton and Storrow's experiment and L/D varies from 6 to 8.5 in Verschoor and Schuit's experiments), the thermal entrance length effect on the average Nusselt numbers may be negligibly small. Thus, the average Nusselt number predicted from the present analysis for a fully developed flow can be compared with the experimental results presented in refs. [19, 20].

For this purpose, computations for the Nusselt numbers given by equations (56) and (63) corresponding to the experimental conditions were carried out with $\omega = 1.5$ and $D_T = 0.17$. These values of ω and D_T were determined recently by Cheng *et al.* [15] by matching both the predicted temperature distribution and the Nusselt number with experimental data for forced convection of water in a thermally developing flow through a packed channel with asymmetric heating [15]. For comparison purposes, computations of equations (56) and (63) were also carried out without a wall function ($\omega = 0$). It was found that with the values of $\omega = 0$ and $D_T = 0.05$, the predicted Nusselt numbers are also in reasonable agreement with experimental data, as will be discussed below. These findings confirm our previous experience that for a given value of ω, one can find a value of D_T such that the predicted Nusselt numbers would match with experimental data. However, different values of ω would give different radial temperature distributions (see below for further discussion). Thus, a unique set of values ω and D_T can only be determined by matching both the radial temperature and surface heat flux data.

Figure 3 is a comparison of the experimentally determined Nusselt numbers [19] and the predicted Nusselt numbers (with and without a wall function)

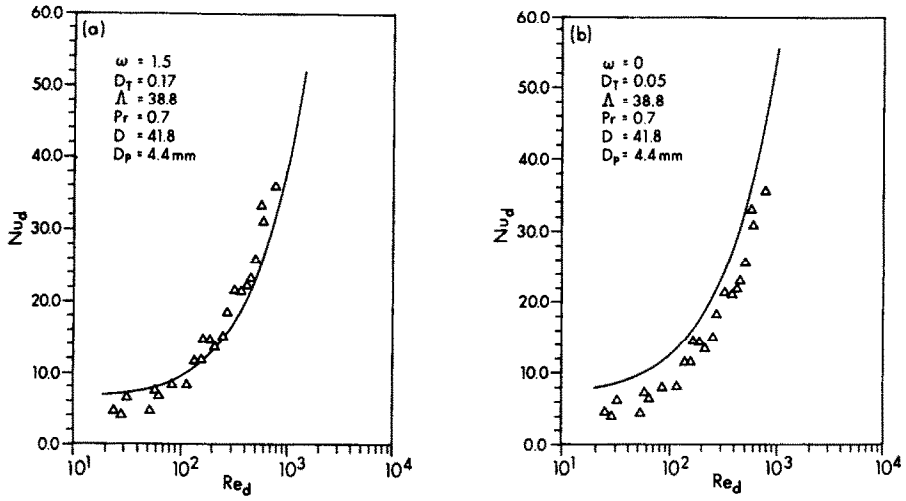

FIG. 3. Comparison of predicted Nusselt numbers with experimental results [19] for a packed tube with constant heat flux: (a) with wall function; (b) without wall function.

in a packed tube with constant heat flux. Similar comparisons of results for forced convection in two different sizes of packed tubes ($D = 43$ and 50 mm) with constant wall temperature are presented in Figs. 4 and 5. In Fig. 4 the predicted Nusselt numbers are computed with a wall function ($\omega = 1.5$ and $D_T = 0.17$) while in Fig. 5 the predicted Nusselt numbers are computed without a wall function ($\omega = 0$ and $D_T = 0.05$). It is seen from Figs. 3–5 that with the exception of the case of $D = 50$ mm and $d_p = 8$ mm in Fig. 4(b), the predicted Nusselt numbers with a wall function are in better agreement with experimental data.

Numerical results for the dimensionless radial temperature distributions at different values of Re_d and γ are presented in Fig. 6 for the case of constant heat flux, and in Fig. 7 for the case of constant wall temperature. The solid lines in these figures represent the computed radial temperature distributions with a wall function ($\omega = 1.5$ and $D_T = 0.17$) while the dashed lines are those without a wall function ($\omega = 0$ and $D_T = 0.05$). As shown in these figures, the differences in the predicted radial temperature distributions with or without a wall function are small for low Reynolds numbers ($Re_d < 100$) or for low values of γ (e.g. $\gamma = 0.03$). However, for high Reynolds numbers or high values of γ, there are marked differences in the shape of the radial temperature profile with or without a wall function. Further, it is shown in these figures that with a wall function the predicted temperature profiles are flatter and the predicted wall temperature gradients are steeper than those without a wall function; and that these effects are more pronounced as the Reynolds number is increased. Unfortunately, since no radial temperature data were taken by Quinton and Storrow [19] or by Verschoor and Schuit [20],

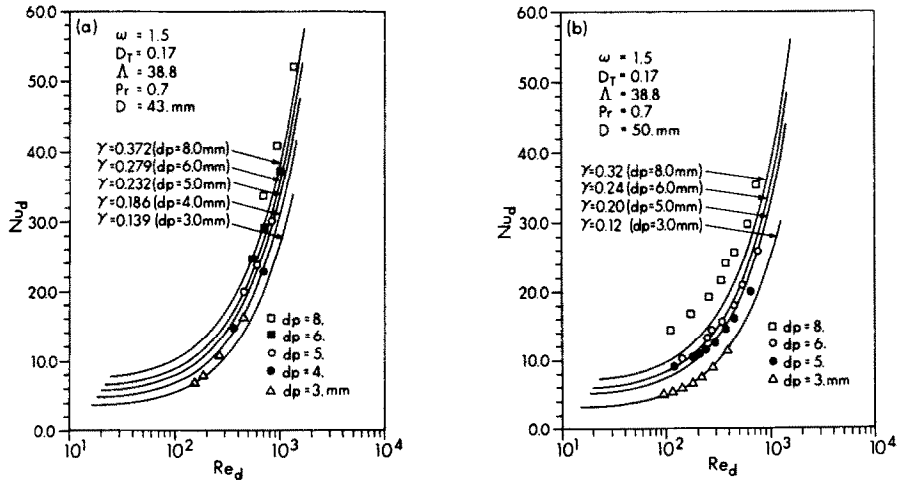

FIG. 4. Comparison of predicted Nusselt numbers based on $\omega = 1.5$ and $D_T = 0.17$ with experimental results [20] for two packed tubes with constant wall temperature: (a) $D = 43$ mm; (b) $D = 50$ mm.

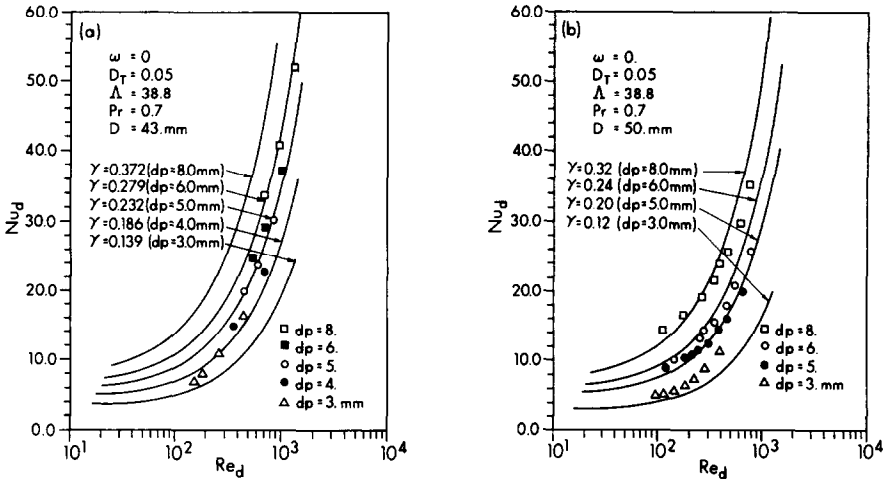

FIG. 5. Comparison of predicted Nusselt numbers based on $\omega = 0$ and $D_T = 0.05$ with experimental results [20] for two packed tubes with constant wall temperature: (a) $D = 43$ mm; (b) $D = 50$ mm.

a comparison with experimental data cannot be made. In comparison of Figs. 5 and 6, it is shown that the value of γ and the wall function have smaller effects for the case of constant heat flux than that of constant wall temperature. At high Reynolds numbers, the dimensionless radial temperature profile (and consequently the Nusselt number) becomes relatively independent of the thermal boundary conditions at the wall.

4. CONCLUDING REMARKS

The fluid flow and heat transfer characteristics of a fully-developed forced convective flow in a cylindrical packed tube heated circumferentially with constant heat flux or constant wall temperature are analyzed in this paper. The effects of non-Darcy and variable porosity are taken into consideration in the momentum equation, while the effects of transverse thermal dispersion and variable stagnant thermal conductivity are taken into consideration in the energy equation. However, the dispersion viscosity effect is neglected in the momentum equation. This is because no model is presently available to take into consideration this effect which is expected to be small. It was found that if the values of $\omega = 1.5$ and $D_T = 0.17$ (determined in a previous paper) are used in the expressions for the transverse thermal dispersion conductivity, the predicted Nusselt numbers agree with the experimental data. It is relevant to note that if no wall function is introduced and if the values of $\omega = 0$ and $D_T = 0.05$ are used in the computations of the energy equation, the predicted Nusselt numbers also agree reasonably well with experimental data. However, the shape of the temperature profiles, with or without a wall function, is markedly different from each other. This is especially true at high Reynolds numbers or at high particle to tube diameter ratios. These findings confirm our previous experience that the validity of the wall function concept for modeling the wall effect on the transverse thermal dispersion process can only be assessed from experiments in which both the surface

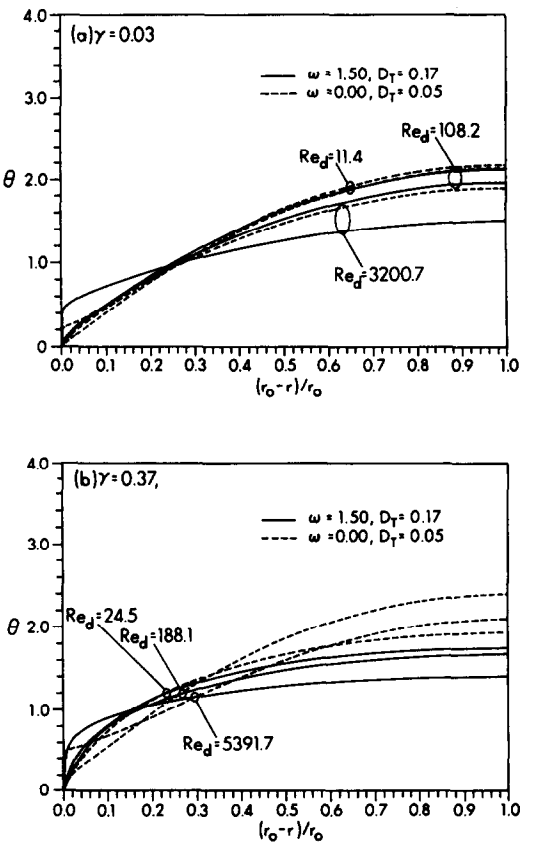

FIG. 6. Predicted dimensionless radial temperature profiles in a packed tube with constant heat flux: (a) $\gamma = 0.03$; (b) $\gamma = 0.37$.

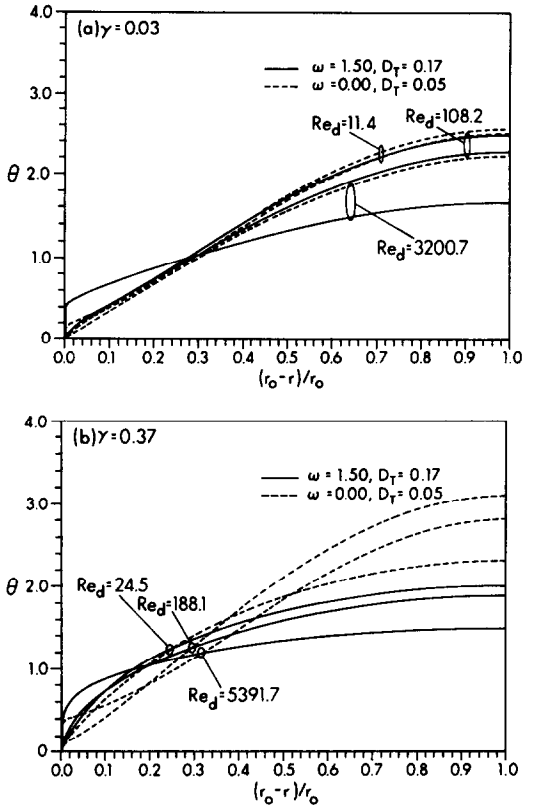

FIG. 7. Predicted dimensionless radial temperature profiles in a packed tube with constant wall temperature: (a) γ = 0.03; (b) γ = 0.37.

heat flux and radial temperature distributions are measured simultaneously.

It must be emphasized that there are a large number of empirical constants used in the present analysis. Thus, the computed heat transfer characteristics depend not only on the values of ω and D_T but also on the values of a, b, C_1 and N_1 used in the computations of velocity distribution. At the present time, there exist considerable uncertainties in the value of a, b, C_1 and N_1. If any of these values is changed, the values of ω and D_T must be modified in order to match with experimental data. For example, if $N_1 = 5$ is used in the computation of the velocity distribution, the values of $D_T = 0.12$ and $\omega = 1.1$ should be used so that the predicted heat transfer characteristics would match with experimental data.

Acknowledgement—This work was supported by NSF through Grant No. CBT83-12095.

REFERENCES

1. J. Beck, Design of packed catalytic reactors. In *Advances in Chemical Engineering* (Edited by T. B. Drew, J. W. Hoopes, Jr. and T. Vermeulen), Vol. 3, pp. 203–270. Academic Press, New York (1962).
2. V. Hlaveck and J. Votruba, *Chemical Reactor Theory: a Review* (Edited by L. Lapidus and N. Amundson). Chap. 6. Prentice-Hall, Englewood Cliffs, New Jersey (1977).
3. D. G. Brunnell, H. B. Irvin, R. W. Oslon and J. M. Smith, Effective thermal conductivities in gas–solid systems, *Ind. Engng Chem.* **41,** 1977–1981 (1949).
4. W. Brotz, Untersuchungen uber warmeleitung, stofftransport und druckabfall in durchstromten schuttgutern, *Chemie-Ingr-Tech.* **23,** 408–416 (1951).
5. C. A. Coberly and W. R. Marshall, Jr., Temperature gradients in gas streams flowing through fixed granular beds, *Chem. Engng Programs* **47,** 141–150 (1951).
6. R. E. Chao, R. A. Caban and M. M. Irizarry, Wall heat transfer to chemical reactors, *Can. J. Chem. Engng* **51,** 67–70 (1973).
7. W. R. Paterson and J. J. Carberry, Fixed bed catalytic reactor modelling, *Chem. Engng Sci.* **38,** 175–180 (1983).
8. S. S. Kwong and J. M. Smith, Radial heat transfer in packed beds, *Ind. Engng Chem.* **49,** 894–903 (1957).
9. B. A. Finlayson, Packed bed reactor analysis by orthogonal collocation, *Chem. Engng Sci.* **26,** 1081–1091 (1971).
10. J. S. M. Botterill and A. O. O. Denloye, A theoretical model of heat transfer to a packed or quiescent fluidized bed, *Chem. Engng Sci.* **33,** 509–515 (1978).
11. M. Ahmed and R. W. Fahien, Tubular reactor design—I, *Chem. Engng Sci.* **27,** 567–576 (1972).
12. P. Cheng and D. Vortmeyer, Transverse thermal dispersion and velocity profiles of convective flow through a packed bed, *Chem. Engng Sci.* (1987), in press.
13. P. Cheng and C. T. Hsu, Fully-developed, forced convective flow through an annular packed-sphere bed with wall effects, *Int. J. Heat Mass Transfer* **29,** 1843–1853 (1986).
14. P. Cheng and C. T. Hsu, Applications of Van Driest's mixing length theory to transverse thermal dispersion in a packed bed with bounding walls, *Int. Commun. Heat Mass Transfer* **13,** 613–625 (1986).
15. P. Cheng, C. T. Hsu and A. Chowdhury, Wall effects on transverse thermal dispersion in the forced convective flow in the entrance region of a packed channel with asymmetric heating, submitted for publication (1987).
16. K. Schroeder, V. Renz and K. Elegeti, *ForschBer. Landes NRhein-Westf.* 3037 (1981).
17. S. Yagi and D. Kunii, Studies on heat transfer near wall surface on packed beds, *A.I.Ch.E. Jl* **6,** 97–104 (1960).
18. K. Vafai and C. L. Tien, Boundary and inertia effects on flow and heat transfer in porous media, *Int. J. Heat Mass Transfer* **24,** 195–203 (1981).
19. J. H. Quinton and J. A. Storrow, Heat transfer to air flowing through packed tubes, *Chem. Engng Sci.* **5,** 245–257 (1956).
20. H. Verschoor and G. C. A. Schuit, Heat transfer to fluids flowing through a bed of granular solids, *Appl. Scient. Res.* **A2,** 97–119 (1952).
21. D. Vortmeyer and J. Schuster, Evaluation of steady flow profiles in rectangular and circular packed beds by a variational method, *Chem. Engng Sci.* **38,** 1691–1699 (1983).
22. S. Ergun, Fluid flow through packed columns, *Chem. Engng Progress* **48,** 89–94 (1952).
23. M. D. Van Dyke, *Perturbation Methods in Fluid Mechanics.* Academic Press, New York (1964).
24. W. M. Kays and M. E. Crawford, *Convective Heat and Mass Transfer.* McGraw-Hill, New York (1980).
25. P. Zehner and E. U. Schluender, Waermeleitfahigkeit von schuettungen bei massigen temperaturen, *Chemie-Ingr-Tech.* **42,** 933–941 (1970).

EFFETS DE LA DISPERSION THERMIQUE TRANSVERSALE SUR LA CONVECTION FORCEE ETABLIE DANS LES LITS FIXES CYLINDRIQUES

Résumé—On étudie les caractéristiques de l'écoulement forcé et du transfert thermique dans un lit fixe tubulaire avec chauffage symétrique. On utilise le modèle Darcy–Brinkman–Ergun avec variation radiale de la porosité approchée par une fonction exponentielle. On construit une solution composite pour le profil de vitesse axiale d'écoulement hydrodynamiquement établi. Est illustrée l'interaction des effets d'inertie et de paroi sur la perte de charge et sur le profil de vitesse radiale. Les effets de la dispersion transversale et de la conductivité thermique variable sont pris en compte dans l'équation de l'énergie pour un écoulement thermiquement développé dans le lit cylindrique qui est chauffé à flux constant ou à température constante sur la circonférence. Le concept de longueur de mélange est utilisé pour modéliser l'effet de la paroi sur le mécanisme de dispersion thermique transverse et les nombres de Nusselt calculés s'accordent bien avec les données expérimentales existantes. Des résultats numériques sur les caractéristiques du transfert thermique dans les colonnes fixes sans introduire le concept de longueur de mélange sont aussi présentés pour permettre une comparaison.

EINFLUSS DES QUERGERICHTETEN WÄRMETRANSPORTES AUF DIE VOLL-ENTWICKELTE ERZWUNGENE KONVEKTION IN ZYLINDRISCHEN FÜLLKÖRPERSÄULEN

Zusammenfassung—Strömung und Wärmeübergang in einer voll-entwickelten erzwungenen Konvektionsströmung in einer zylindrischen Füllkörpersäule mit symmetrischer Beheizung werden untersucht. Das Darcy–Brinkman–Ergun-Modell wird als Impulsgleichung benutzt, wobei die radiale Veränderung der Porosität in der Füllkörperkolonne durch eine Exponentialfunktion näherungsweise beschrieben wird. Die gekoppelte Auswirkung von Trägheit und Kanalbildung an der Wand auf den Druckabfall und das axiale Geschwindigkeitsprofil wird gezeigt. Die Einflüsse des quergerichteten Wärmetransportes und der veränderlichen Wärmeleitfähigkeit im Ruhezustand werden in der Energiegleichung für die thermisch voll-entwickelte Strömung in der Füllkörpersäule berücksichtigt. Die Beheizung erfolgt am Umfang mit konstanter Wärmestromdichte oder konstanter Wandtemperatur. Das Verfahren der Mischungslänge wird verwendet, um die Wandeffekte auf den quergerichteten Wärmetransport wiederzugeben. Die berechneten Nusselt-Zahlen stimmen gut mit vorliegenden Versuchsergebnissen überein. Zum Vergleich werden auch numerische Ergebnisse ohne Einführen des Mischungsweg-Ansatzes vorgestellt.

ВЛИЯНИЕ ПОПЕРЕЧНОЙ ТЕПЛОПРОВОДНОСТИ НА ПОЛНОСТЬЮ РАЗВИТУЮ ВЫНУЖДЕННУЮ КОНВЕКЦИЮ В ЦИЛИНДРИЧЕСКИХ КОЛОННАХ С ВНУТРЕННИМИ НАСАДКАМИ

Аннотация—Проведен анализ характеристик течения и теплообмена при полностью развитой вынужденной конвекции в симметрично нагреваемой цилиндрической трубе с внутренними насадками. В качестве уравнения количества движения использовалась модель Дарси–Бринкмана–Эргуна, а радиальное изменение пористости заполнителя в колонне аппроксимировалось с помощью экспоненциальной функции. При построении решения для аксиального профиля скорости гидродинамически полностью развитого течения применен метод сращиваемых асимптотических разложений. Показано влияние взаимодействия инерционных и пристеночных эффектов на перепад давления и профиль аксиальной скорости. В уравнении энергии для термически полностью развитого течения в колонне с заполнителем при постоянном по периметру тепловом потоке или при постоянной температуре стенки учтены эффекты поперечной теплопроводности и переменных значений коэффициента теплопроводности в стационарном случае. Используется понятие длины смешения для моделирования влияния пристенных эффектов на поперечную теплопроводность. Установлено, что теоретические числа Нуссельта согласуются с имеющимися экспериментальными данными. Для сравнения приводятся также результаты численного исследования соответствующих теплообменных характеристик в колоннах с заполнителем, когда концепция длины смешения не использовалась.